Biochemical Pharmacology 223 (2024) 116188

Contents lists available at ScienceDirect

Biochemical Pharmacology

journal homepage: www.elsevier.com/locate/biochempharm

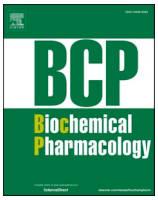

Targeted mutagenesis of negatively charged amino acids outlining the substrate translocation path within the human organic cation transporter 3

Kyra-Elisa M. Redeker [a,*], Sophie Schröder [b], Christof Dücker [a], Jürgen Brockmöller [a], Lukas Gebauer [a]

[a] Institute of Clinical Pharmacology, University Medical Center Göttingen, D-37075 Göttingen, Germany
[b] Department for Epigenetics and Systems Medicine in Neurodegenerative Diseases, German Center for Neurodegenerative Diseases (DZNE), D-37075 Göttingen, Germany

ARTICLE INFO

Keywords:
Organic cation transporter 3
SLC22A3
Site-directed mutagenesis
Substrate binding
Transport mechanism

ABSTRACT

Recently published cryo-EM structures of human organic cation transporters of the SLC22 family revealed seven, sequentially arranged glutamic and aspartic acid residues, which may be relevant for interactions with positively charged substrates. We analyzed the functional consequences of removing those negative charges by creating D155N, E232Q, D382N, E390Q, E451Q, E459Q, and D478N mutants of OCT3.

E232Q, E459Q, and D478N resulted in a lack of localization in the outer cell membrane and no relevant uptake activity. However, D155N and E451Q showed a substrate-specific loss of transport activity, whereas E390Q had no remaining activity despite correct membrane localization. In contrast, D382N showed almost wild-type-like uptake. D155 is located at the entrance to the substrate binding pocket and could, therefore be involved in guiding cationic substrates towards the inside of the binding pocket. For E390, we confirm its critical function for transporter function as it was recently shown for the corresponding position in OCT1. Interestingly, E451 seems to be located at the bottom of the binding pocket in the outward-open confirmation of the transporter. Substrate-specific loss of transport activity of the E451Q variant suggests an essential role in the transport cycle of specific substances as part of an opportunistic binding site.

In general, our study highlights the impact of the cryo-EM structures in guiding mutagenesis studies to understand the molecular level of transporter-ligand interactions, and it also confirms the importance of testing multiple substrates in mutagenesis studies of polyspecific OCTs.

1. Introduction

Solute carrier membrane transporters regulate the movement of hydrophilic endogenous and exogenous substances across lipid bilayers of biological membranes. The organic cation transporters (OCT) 1, 2, and 3 are polyspecific transporters with broad substrate selectivity [1]. They transport mainly hydrophilic, positively charged substances with a molecular weight between 150 and 450 Da [2–4], although uptake has been described in exceptional cases for uncharged or even negatively charged substances [5]. All three OCTs transport most substrates but with a varying degree of preference [4].

OCT1 and OCT2 are mainly expressed in liver [6,7], and kidneys [8], respectively. OCT3 has a broad expression pattern found in the brain [9], the heart [10], the liver [7] and the lungs [11]. The most relevant physiological role of OCT3 is not well understood, although there is evidence that OCT3 is involved in monoamine neurotransmitter mediated signal transmission in the brain [12], contractility of the heart [13], and also thermogenesis in adipose tissue [14]. Besides this, OCT3 may be involved in liver fibrosis [15] and the progression of hepatocellular carcinoma [16]. It may also be involved in different psychiatric diseases

Abbreviations: ASP^+, 4-(4-(dimethylamino)styryl)-*N*-methylpyridinium; BSA, bovine serum albumin; Cl_{int}, intrinsic clearance; Cryo-EM, cryogenic electron microscopy; DMEM, Dulbecco's Modified Eagles Medium; D-PBS, Dulbecco's phosphate buffered saline; EV, empty vector; HBSS, Hank's balanced salt solution; HPLC-MS/MS, high-performance liquid chromatography coupled to tandem mass spectrometry; m-IBG, *meta*-iodobenzylguanidine; MPP^+, 1-Methyl-4-phenylpyridinium; NGS, normal goat serum; OAT, organic anion transporter; OCT, organic cation transporter; OCTN, Organic cation transporters novel; PCR, polymerase chain reaction; SEM, standard error of the mean; WT, wild type.

* Corresponding author at: Institute of Clinical Pharmacology, University Medical Center Göttingen, Georg-August University, Robert-Koch-Str. 4037075 Göttingen, Germany.

E-mail address: kyra-elisamaria.redeker@med.uni-goettingen.de (K.-E.M. Redeker).

https://doi.org/10.1016/j.bcp.2024.116188
Received 20 December 2023; Received in revised form 12 March 2024; Accepted 2 April 2024
Available online 3 April 2024

[17].

OCTs are proteins with 12 membrane-spanning helices and intracellular N- and C-terminal loops. According to the current understanding of the transport mechanism, OCTs follow an alternating cycle of outward-open via outward- and inward-occluded to inward-open states [18]. Until 2022, studies on OCT function were mainly based on homology modelling and thereof based targeted mutagenesis studies [19]. Most studies were on OCT1, and many studied the rat orthologue [20–22]. The profound polyspecificity is a characteristic of OCTs, particularly of OCT1, and impedes the understanding of OCT-ligand interactions [23]. One explanation for OCTs polyspecificity would be that structurally different substrates might bind to different sites within the transporter. Indeed, multiple studies suggest different partially overlapping binding sites for different substrates [19,24,25]. Most studies also agreed on a critical role of a negatively charged aspartate (D474, codon numbering of OCT1) in transmembrane domain 11 [5,22,26–28]. This conception was supported by the fact that this aspartate is conserved between all OCTs whereas for the related zwitterion (OCTNs, organic cation transporters novel) and anion transporters (OATs, organic anion transporters), a positively charged arginine is located at this position [1].

Recently published studies using cryogenic electron microscopy (cryo-EM) provided the first experimentally derived structures for OCTs [29–31]. Generally, they support the alternating access model of OCTs and have additionally pointed out the critical role of other negatively charged amino acids for the transport via OCTs. As shown for OCT1 [30], E386A (corresponds to E390 in OCT3) was even more disruptive for transporting a model substrate as the D474A mutation. A study on OCT3 revealed that several negatively charged amino acids are located along the translocation pathway, contributing to an anionic surface which likely attracts the cationic ligand: D155, E232, D382, E390, E451, E459, and D478 (Fig. 1A) [29]. Moreover, they illustrated that in the anion transporter OAT1, the opposite was the case. Models of OAT1 were characterized by a cationic surface in the corresponding area which aligns with its substrate specificity for anionic substrates [29]. So far, there is no functional data on the role of these amino acids available. Except E451, all of these amino acids are conserved among the three OCTs, and some are even conserved for the related zwitterionic transporters OCTNs or even the organic anion transporters (OATs) of the SLC22 gene family (Fig. 1B).

In this study, we selectively mutated those amino acids, aspartate to asparagine and glutamate to glutamine, to remove the negative charges proposed to be relevant for substrate binding and transport. We analyzed the membrane localization and then performed functional characterization of the uptake by and inhibition of these transporter variants. This study sheds light on several non-studied amino acids and by this, should improve the molecular understanding of ligand-OCT3 interactions.

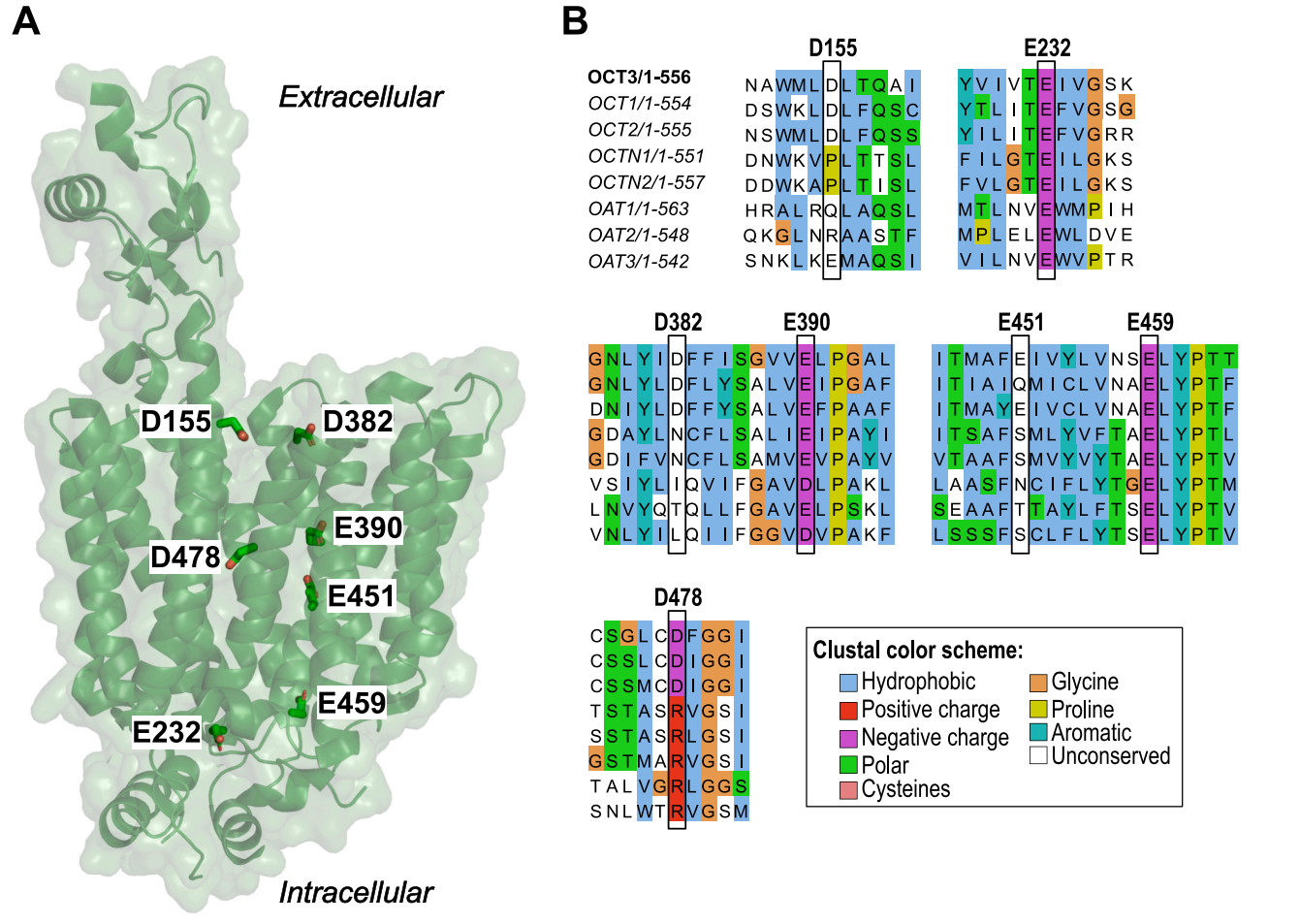

Fig. 1. OCT3 structure and here investigated amino acids. A: The apo structure of human OCT3 in an outward-open confirmation according to the study of Khanppnavar et al. [29] deposited in the protein data bank (ID: 7ZH0). The structure and the amino acids studied here were visualized with Pymol. **B:** Sequence alignment of SLC22 transporters. Sequence alignment with sequences from UniProt [32] was done using the MUSCLE algorithm [33]. Visualization was performed with Jalview [34], and positions were colored using the Clustal color scheme.

2. Materials and methods

2.1. Site-directed mutagenesis

The cDNA of OCT3 (pDONR221-SLC22A3_STOP) was purchased from RESOLUTE Consortium & Giulio Superti-Furga (Addgene plasmid #161190; https://n2t.net/addgene:161190; RRID: Addgene_161190). OCT3 was re-cloned into the pcDNA5/FRT vector (Thermo Fisher Scientific, Darmstadt, Germany) via restriction enzyme digestion cloning using NheI-HF and NotI-HF (New England Biolabs, Frankfurt am Main, Germany). The primers used for amplification of OCT3 are listed in Table 1 and they have integrated the restriction sites for NheI and NotI. After the transformation into OneShot TOP10 electrocompetent *E. Coli* (Thermo Fisher Scientific, Darmstadt, Germany) via electroporation, the correct sequence of the reading frame was validated via Sanger Sequencing.

The introduction of point mutations (D155N, E232Q, D382N, E390Q, E451Q, E459Q, and D478N) into the plasmid pcDNA5::hOCT3 was performed individually for each mutation by site-directed mutagenesis using a protocol designed with two single-primer reactions in parallel [35]. This was done to avoid primer-primer annealing. The PCR was composed of 2.5 µl 10 × KOD buffer (KOD Hot Start DNA Polymerase Kit; Merck, Darmstadt, Germany), 5 µl Q-solution (Qiagen, Hilden, Germany), 2.5 µl dNTPs (each 2 mM; Thermo Fisher Scientific, Darmstadt, Germany), 1 µl $MgSO_4$ (25 mM; Merck, Darmstadt, Germany), 0.65 µl of the respective forward or reverse mutagenesis primer (Table 1), 0.5 µl HotStart KOD polymerase, 6.25 µl DNA (80 ng/µl) and 6.6 µl double-distilled water. After heating the PCR mixture to 95 °C for 3 min, a PCR cycle of 95 °C for 30 s, 66 °C for 30 s and 72 °C for 4 min was repeated 30 times and then held at 72 °C for 10 min. Then, the PCR products of the matching forward and reverse primers were mixed. After denaturing the mixture at 95 °C for 5 min, it was slowly cooled down at 90 °C for 1 min, 80 °C for 1 min, 70 °C for 30 s, 60 °C for 30 s, 50 °C for 30 s and 40 °C for 30 s. Next, the PCR products were digested with 2 µl DpnI (20 U/µl; New England Biolabs, Frankfurt am Main, Germany) using 6 µl rCut smart buffer (New England Biolabs) and they were incubated at 37 °C overnight. On the next day, the digested product was dialysed and transformed into OneShot TOP10 electrocompetent *E. Coli* (Thermo Fisher Scientific, Darmstadt, Germany) via electroporation using a Gene Pulser II (Bio-Rad Laboratories, Hercules, California, USA). The correct sequence was validated via Sanger Sequencing and cloned into a new pcDNA5/FRT vector via restriction enzyme digestion cloning before stable transfection into HEK293 cells.

2.2. Stable transfection of wild-type and mutated OCT3-overexpressing cell lines

The HEK293 cells overexpressing OCT3 WT or with a mutation were generated via stable transfection using the recombinant site-specific FlpIn system (Thermo Fisher Scientific, Darmstadt, Germany). Empty vector-transfected control cells were generated as described previously [36]. Twenty-four hours before transfection, 1 × 10^6 HEK293 T-REx cells were seeded on a 6-well plate with standard cell culture medium consisting of Dulbecco's Modified Eagles Medium (DMEM) supplemented with 10 % FBS as well as penicillin (100 U/ml) and streptomycin (100 µg/ml); purchased from Thermo Fisher Scientific, Darmstadt,

Table 1
Primers used for the generation and validation of OCT3 variants.

Primers for restriction enzyme cloning of OCT3 into pcDNA5/FRT vector			
Enzyme	Direction	Sequence (5→3) with restriction site	
NheI	forward	AAAAAGCAGCTAGCACCATGCCTAGCTTTGACGAG	
NotI	reverse	GCTGGGTCGCGGCCGCTTACAGGTGAGAGCGGGA	
Primers for site-directed mutagenesis			
OCT3 Mutation	Direction	Sequence (5→3)	
D155N	forward	GAACGCCTGGATGCTG**AAT**CTGACACAGGCCATCC	
	reverse	GGATGGCCTGTGTCAG**ATT**CAGCATCCAGGCGTTC	
E232Q	forward	TACGTGATCGTGACC**CAG**ATCGTGGGCTCCAAGCAG	
	reverse	CTGCTTGGAGCCCACGAT**CTG**GGTCACGATCACGTA	
D382N	forward	GCAACCTGTATATC**AAT**TTCTTTATCAGCGGAGTG	
	reverse	CACTCCGCTGATAAAGAA**ATT**GATATACAGGTTGC	
E390Q	forward	ATCAGCGGAGTGGTG**CAG**CTGCCAGGCGCCCTGCTG	
	reverse	CAGCAGGGCGCCTGGCAG**CTG**CACCACTCCGCTGAT	
E451Q	forward	ATCACAATGGCCTTT**CAG**ATCGTGTACCTGGTG	
	reverse	CACCAGGTACACGAT**CTG**AAAGGCCATTGTGAT	
E459Q	forward	TACCTGGTGAACTCC**CAG**CTGTATCCCACCACACTG	
	reverse	CAGTGTGGTGGGATACAG**CTG**GGAGTTCACCAGGTA	
D478N	forward	GTGCTCTGGCCTGTGC**AAT**TTCGGCGGCATCATCG	
	reverse	CGATGATGCCGCCGAA**ATT**GCACAGGCCAGAGCAC	
Primers for genomic validation			
PCR	Primer	Sequence (5→3)	Amplicon size [bp]
Integration PCR	P_{SV40}	AGCTGTGGAATGTGTGTCAGTTAGG	519
	P_{Hyg_r2}	ACGCCCTCCTACATCGAAGCTGAAA	
Multiple Integration PCR	P_{FRT_f}	AATCGGGGGCTCCCTTTAGGGTTCC	214
	P_{Hyg_r2}	ACGCCCTCCTACATCGAAGCTGAAA	
Gene-of-interest PCR	P_{CMV}	CCATGGTGATGCGGTTTTGGCAGTA	3131
	P_{LacZ}	CCTTCCTGTAGCCAGCTTTCATCAA	
Primers for quantitative real-time PCR			
Gene	Direction	Sequence (5→3)	Amplicon size [bp]
HPRT1	forward	TGACACTGGCAAAACAATGCA	94
	reverse	GGTCCTTTTCACCAGCAAGCT	
OCT3	forward	TCGGCGGCAACCTGTATATC	86
	reverse	TCTCTCGATGGTCAGCAGGA	
Primers for eGFP-OCT3 fusion protein			
Gene	Direction	Sequence (5→3)	
eGFP	forward	AAAAAGCAGCTAGCACCATGGTGAGCAAGGGCGAGG	
	reverse	TCAAAGCTAGGCATCTTGTACAGCTCGTCCATGCCG	
OCT3	forward	GACGAGCTGTACAAGATGCCTAGCTTTGACGAGGCCC	
	reverse	GCTGGGTCGCGGCCGCTTACAGGTGAGAGCGGGA	

Germany. For transfection, one tube contained 12 µl FuGene6 transfection reagent diluted in 100 µl pure DMEM. In a second tube, 0.4 µg plasmid DNA, as well as 3.6 µg pOG44 helper plasmid, were added to 100 µl pure DMEM. After 5 min, the DNA mixture was added to the transfection reagent and incubated for another 15 min. Meanwhile, the cells were washed once with cell culture DMEM medium supplemented with 10 % FBS. Then, the transfection mixture was added dropwise to cells covered in 1.8 ml cell culture medium with 10 % FBS and incubated overnight. After 24 h, the transfection medium was exchanged to standard cell culture medium consisting of DMEM, 10 % FBS and penicillin/streptomycin. Further 24 h later, the cells were transferred to a 100 mm cell culture dish by careful resuspension with medium and incubated overnight. The next day, the selection antibiotic Hygromycin B (Thermo Fisher Scientific, Darmstadt, Germany) was added to the cells dropwise to a concentration of 300 µg/ml. Single colonies were selected after nine to ten days, transferred to a 24-well plate and incubated with a reduced concentration of Hygromycin B of 50 µg/ml. The cells were transferred to 6-well and further to T25 flasks when a confluence of 70–80 % was reached. Cell samples for DNA and RNA isolation were collected during the early passages of the cells.

2.3. Genomic validation of generated cell lines

The vector's correct integration into overexpressing-cell lines was validated via three independent PCRs (Fig. 2A and B). The integration PCR confirmed the integration of the vector into the host genome (519 bp), and the multiple-integration-PCR ensured that the vector has not inserted multiple times (214 bp). The presence of gene-of-interest was verified with a third PCR (3131 bp).

Genomic DNA was isolated from 2 × 10^6 cells using the QIAGEN DNeasy Blood and Tissue Kit (Qiagen, Hilden, Germany) according to the manufacturer's protocol. The integration and the multiple integration PCR were performed with the QIAGEN Multiplex PCR Kit (Qiagen, Hilden, Germany) consisting of 5 µl of 2 × QIAGEN Multiplex PCR master mix, 2 µl of Q-solution, respectively 0.25 µl of 10 µM forward and reverse primer (Table 1), 1 µl of isolated genomic DNA (100 ng/µl) and 1.5 µl double-distilled water. After heating the PCR mixture to 95 °C for 15 min, a cycle of 95 °C for 30 s, 62.7 °C for 1:30 min and 72 °C for 1:30 min cycled for 35 times before a temperature of 72 °C was held for 10 min to complete the reaction. As positive control for the PCR, a cell clone was used that showed an integration and multiple integration of the respective plasmid into the genome. For a correct integration of a plasmid, a positive outcome is expected for the integration PCR but a negative outcome for the multiple integration PCR.

The gene-of-interest PCR is used to detect the presence of the gene-of-interest using gene-unspecific primers surrounding the gene locus. For this, the Expand Long Template PCR-system (Roche Diagnostics, Mannheim, Germany) was used containing 2.8 µl 10 × Expand Long buffer, 5.6 µl Q-solution (Qiagen, Hilden, Germany), 4.5 µl dNTPs (each 2 mM; Thermo Fisher Scientific, Darmstadt, Germany), 1.5 µl $MgSO_4$ (25 mM; Merck, Darmstadt, Germany), 0.5 µl of 10 µM forward and reverse primer respectively (see Table 1), 0.3 µl Expand Long polymerase mix, 3 µl DNA (80 ng/µl) and 9.3 µl double-distilled water. The PCR protocol included 94 °C for 2 min, a cycle of 96 °C for 10 s, 60 °C for 20 s and 68 °C for 5 min for 35 rounds, and finally 68 °C for 7 min. The empty pcDNA5 vector was used as a negative control of the gene-of-interest PCR.

2.4. Quantification of gene expression

The gene expression of OCT3 was quantified using quantitative real-time PCR with isolated RNA from cells at three different passages. RNA was isolated from 2 × 10^6 cells using the QIAGEN RNeasy Plus Mini Kit (Qiagen, Hilden, Germany) according to the manufacturer's protocol. In preparation for this, cells were centrifuged at 400 × g for 4 min, and the cell pellet was resuspended in 350 µl RLT lysis buffer supplemented with 1 % beta-mercaptoethanol (v/v; Sigma-Aldrich, Darmstadt, Germany). After RNA isolation, the Superscript II Reverse Transcriptase Kit (Thermo Fisher Scientific, Darmstadt, Germany) was used for cDNA synthesis of 3 µg RNA diluted in 17.75 µl RNase free water. After addition of 1 µl of 10 µM anchored dT primer (5′-TTTTTTTTTTTTTTTTTTVN-3′; Thermo Fisher Scientific, Darmstadt, Germany), the RNA was incubated at 72 °C for 10 min for initiation of primer annealing. Afterwards, the reverse transcription was initiated with addition of 11.25 µl of a mixture containing 6 µl of 5 × Superscript RT buffer, 3.5 µl of 0.1 M dithiothreitol (DTT), 1 µl of dNTPs (each 2 mM), 0.5 µl RNase inhibitor (40 U/µl) and 0.25 µl Superscript II Reverse Transcriptase (200 U/µl). After an incubation period at 42 °C for 1 h, enzyme denaturation was performed at 75 °C for 15 min. Finally, the newly synthesized cDNA was diluted with 70 µl of RNA-free water.

Quantitative real-time PCR was performed in triplicates with 2 µl of 1:10 diluted cDNA (6 ng cDNA) and the HOT FIREPol EvaGreen qPCR Mix Plus Kit (Solis BioDyne, Tartu, Estonia) consisting of 2 µl of 5 × EvaGreen qPCR Mix, 0.4 µl of primer mixture with 10 µM of each forward and reverse primer, and 5.6 µl double-distilled water in a 384-well plate using a Taqman 7900 T (Applied Biosystems, Darmstadt, Germany). The utilized primers are listed in Table 1. The SDS 1.2 software (Applied Biosystems) was used for analysis of qPCR results. The gene expression of OCT3 and its mutants was normalized to the housekeeping gene HPRT1. Additionally, the expression level of mutants was normalized to the wild-type transporter. The cycle threshold values were evaluated using the following equation [37]:

$$relative\ gene\ expression = 2^{-\left(ct_{mutant} - ct_{mutant,HPRT1}\right) - \left(ct_{WT} - ct_{WT,HPRT1}\right)}$$

The selection of mutant clones was made based on a comparable RNA-expression level of all mutants (Fig. 2C).

2.5. Generation of eGFP-hOCT3 fusion proteins and subcellular localization

The fusion eGFP-OCT3 protein was generated for visualization of the subcellular localization of the transporter (Fig. 2D). First single fragments with overlapping ends were generated by PCR and then fused in a two-step assembly PCR.

The single fragment PCRs for eGFP (Clontech Takara Bio, California, USA) and OCT3 were composed of 5 µl of 10 × KOD buffer (KOD Hot Start DNA Polymerase Kit; Merck, Darmstadt, Germany), 10 µl Q-solution (Qiagen, Hilden, Germany), 5 µl dNTPs (each 2 mM; Thermo Fisher Scientific, Darmstadt, Germany), 3 µl $MgSO_4$ (25 mM; Merck, Darmstadt, Germany), each 1.5 µl of 10 mM forward and reverse primer, 1 µl HotStart KOD, 1 µl DNA (100 ng/µl) and 22 µl double-distilled water. The PCR mixture was heated to 95 °C for 2 min, then, a 35x cycle of 95 °C for 30 s, 64.3 °C for 30 s, and 72 °C for 30 s and 1:30 min, for elongation of eGFP and OCT3, respectively. Lastly, the samples were held at 72 °C for 10 min. Afterwards, the first part of the assembly PCR consisting of 5 µl of 10 × KOD buffer, 10 µl Q-solution, 5 µl dNTPs (each 2 mM), 2 µl $MgSO_4$ (25 mM), 5 µl of the eGFP and OCT3, 1 µl HotStart KOD polymerase and 17 µl double-distilled water was initiated using the following PCR conditions: 95 °C for 2 min, a cycle of 95 °C for 30 s, 50 °C for 45 s and 72 °C for 2 min with 20 repetitions, and 72 °C for 10 min. The second part of the assembly PCR was composed of 5 µl of 10 × KOD buffer, 10 µl Q-solution, 5 µl dNTPs (each 2 mM), 2 µl $MgSO_4$ (25 mM), each 1.3 µl of the forward eGFP primer and the reverse OCT3 primer, 1 µl HotStart KOD polymerase, 2 µl of PCR product of first-step assembly PCR, and 22.4 µl double-distilled water. The PCR was performed under the following conditions: 95 °C for 2 min, a cycle of 95 °C for 30 s, 64.3 °C for 45 s and 72 °C for 2:30 min with 35 repetitions, and 72 °C for 10 min. The PCR products were digested with the NheI-HF and NotI-HF (both New England Biolabs, Frankfurt am Main, Germany) and re-cloned into the pcDNA5/FRT vector.

HEK293 T-REx were transiently transfected for visualization of

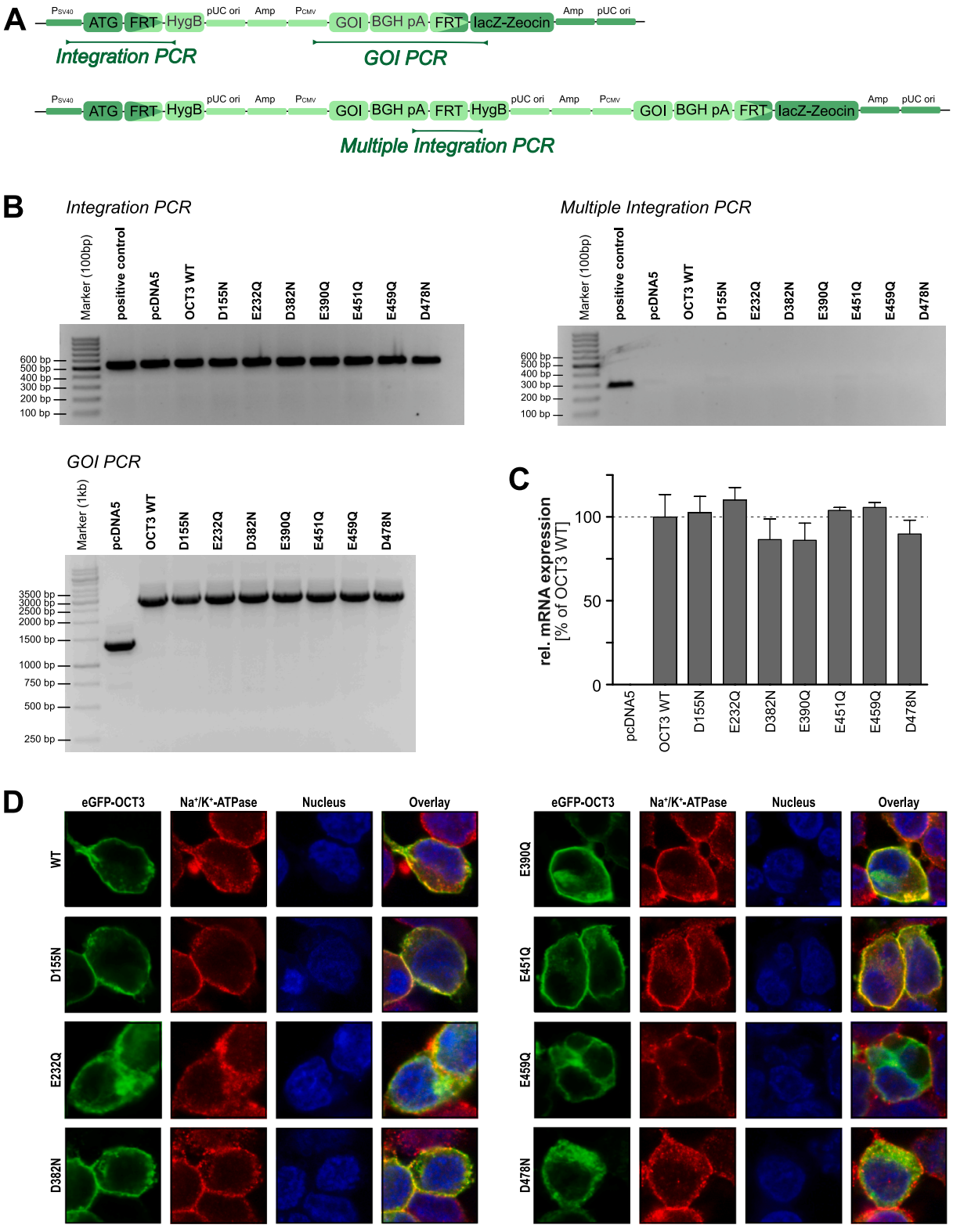

Fig. 2. Validation of generated cell lines. A: Scheme of genomic integration of expression vectors. Shown is a single integrated expression vector and the unwanted event of two sequentially integrated vectors. The three PCRs are highlighted, which were used to validate the correct integration of a single expression vector. **B:** Results of the validation PCRs. Selected clones demonstrated single vector integration. PCR confirmed the presence of the gene of interest (GOI). **C:** Gene expression analysis of OCT3 mutants. Gene expression analysis was done by mRNA quantification by real-time quantitative PCR and normalized to gene expression of wild-type transporter-overexpressing cells. Data is shown as mean ± SEM of three independent mRNA quantifications of different cell passages. **D:** Immunofluorescence localization of OCT3 mutants. eGFP-tagged OCT3 mutants were transiently transfected into HEK293 cells, and membrane localization was determined after staining with an anti-eGFP antibody and comparison to the Na^+/K^+-ATPase as marker of the plasma membrane. Co-localization of the eGFP and Na^+/K^+-ATPase indicates correct membrane localization of the transporter.

subcellular localization using a transfection mixture of FuGene and DNA of eGFP-OCT3 (wild-type and mutants) in a ratio of 3:1. For this, 125,000 cells per well were plated on 4-well Nunc Lab-Tec II Chamber slides (Thermo Fisher Scientific, Darmstadt, Germany) 24 h in advance. For transient transfection, 4.8 µl FuGene6 transfection reagent was diluted in 25 µl pure DMEM in one tube. In a second tube, 1.6 µg plasmid DNA was added to 25 µl pure DMEM. After incubation of 5 min, the tube containing DNA was added to the transfection reagent and incubated for another 15 min. Meanwhile, the cells on the slides were washed once and then covered with 450 µl with cell culture DMEM medium supplemented with 5 % FBS. Finally, the transfection mixture was added dropwise to cells and incubated overnight.

In preparation of immunofluorescence staining, cells were washed twice with Dulbecco's phosphate buffered saline (D-PBS; Thermo Fisher Scientific) and incubated then with 1 µM SYTO Deep Red Nucleic Acid Stain (Thermo Fisher Scientific) dissolved in D-PBS at 37 °C for 30 min. After this, cells were washed twice with D-PBS and fixation was done with 4 % paraformaldehyde for 20 min at room temperature. Afterwards, cells were washed three times with D-PBS and then permeabilised with D-PBS/0.1 % Triton-X (Carl Roth, Karlsruhe, Germany) for 15 min. After two washing steps with D-PBS/0.1 % Tween-20 (Sigma-Aldrich, Darmstadt, Germany), cells were blocked with 0.1 % Tween-20, 1 % bovine serum albumin (BSA) and 20 % normal goat serum (NGS) diluted in D-PBS for 60 min. Next, the primary antibody against eGFP (anti-GFP IgG Alexa Fluor® 488 conjugate, Invitrogen, Thermo Fisher Scientific) and monoclonal mouse anti-Na^+/K^+-ATPase antibody (ab283318; Abcam, Cambridge, United Kingdom) were diluted 1:500 and 1:100, respectively, in D-PBS with 0.1 % Tween-20, 1 % BSA and 5 % NGS and incubated on cells overnight at 4 °C. On the next day, cells were washed four times for 5 min with D-PBS/0.1 % Tween-20 before the secondary antibody polyclonal Alexa Fluor® 594 goat anti-mouse IgG (H + L) (Thermo Fisher Scientific, Darmstadt, Germany) was diluted 1:500 in D-PBS with 0.1 % Tween-20, 1 % BSA and 1.5 % NGS and incubated on cells for 60 min at room temperature. Subsequently, cells were washed again four times for 5 min with D-PBS/0.1 % Tween-20. Finally, the slides were mounted with Roti-Mount FluorCare (Carl Roth) and covered with coverslips. Cells were imaged with a Leica DMi8 microscope (Leica Microsystems, Wetzlar, Germany) that was equipped with a STEDYcon module (Abberior instruments, Göttingen, Germany). Images were taken in confocal mode using a 63 × oil immersion objective with identical acquisition settings for all images.

2.6. In vitro transport experiments

All test compounds for cell experiments were purchased from Sigma-Aldrich (Taufkirchen, Germany), Toronto Research Chemicals (Toronto, ON, Canada) and Santa Cruz Biotechnology (Darmstadt, Germany). General culture conditions for the HEK293 cells used for transport and inhibition experiments were standard cell culture containing Dulbecco's Modified Eagles Medium (DMEM) supplemented with 10 % (v/v) FBS as well as the antibiotics penicillin (100 U/ml) and streptomycin (100 µg/ml). For in vitro transport and inhibition experiments, HEK293 cells overexpressing OCT3 wild type (without eGFP), generated mutants and empty-vector transfected control cells were used.

For in vitro transport experiments, 300,000 cells were plated in 24-well plates pre-coated with poly-D-lysine 48 h in advance. All steps of the transport experiment were performed at 37 °C. Firstly, cells were washed with pre-warmed HBSS+ (Hank's balanced salt solution supplemented with 10 mM HEPES; Thermo Fisher Scientific, Darmstadt, Germany) adjusted to pH 7.4. Then, they were incubated for exactly 2 min with the substrates diluted in pre-warmed HBSS +. The uptake was stopped by adding ice-cold HBSS +. Then, cells were washed twice with ice-cold HBSS + and lysed for 15 min with 80 % (v/v) acetonitrile containing the respective internal standard for eventual mass spectrometry. For each cell line, two wells of cells were lysed in RIPA buffer and total protein content was measured with a bicinchoninic acid assay [38] and compared to standard curves of bovine serum albumin. This was used to normalise uptake data to intraday variations in the number of seeded cells of different cell lines.

2.7. In vitro inhibition experiments

In vitro inhibition experiments were also performed with 300,000 cells in poly-D-lysine pre-coated 24-well plates that were plated 48 h in advance. After a washing step with pre-warmed HBSS+, the 2 µM ASP^+ was incubated simultaneously with and without 20 µM inhibitor for 5 min. Concentration-dependent inhibition of 2 µM ASP^+ were carried out with inhibitor concentrations of 0.01 – 100 µM corticosterone or decynium-22 respectively. A control for passive uptake with empty-vector transfected cells and an un-inhibited control with OCT3-overexpressing cells were incubated with the substrate without inhibitor for the same time. After two washing steps with ice-cold HBSS+, cells were lysed with 80 % (v/v) acetonitrile for 15 min and fluorescence of ASP^+ was measured using a Tecan Ultra Microplate Reader (Tecan Group AG, Männedorf, Switzerland). All ASP^+ measurements were carried out in technical duplicates.

2.8. Concentration analysis

The intracellular drug concentrations of non-fluorescent substances were determined using high-performance liquid chromatography coupled to tandem mass spectrometry (HPLC-MS/MS) analysis. Chromatography was accomplished using a Shimadzu Nexera HPLC System consisting of a CBM-20A controller, a LC-30AD pump, a CTO-20AC column oven and an SIL-30AC autosampler (Shimadzu, Kyoto, Japan). The separation of compounds was performed on a Brownlee SPP RP-Amide column with 4.6 × 100 mm inner dimensions and a particle size of 2.7 µm as well as a preceding Phenomenex C-18 guard column. The mobile phase of reversed-phase chromatography consisted of 0.1 % (v/v) formic acid and an acetonitrile:methanol 6:1 (v/v) organic additive in total concentrations between 3 % and 50 % (v/v) individual for each substance. Detailed chromatographic conditions and mass spectrometric detection parameters were described previously [4,5,39]. Chromatography was carried out at 40 °C with a flow rate of 300 or 400 µl/min. Substances were detected with an API 4000 tandem mass spectrometer (AB SCIEX, Darmstadt, Germany) and quantification of results was performed using the Analyst software (AB SCIEX, version 1.6.2).

Racemic norphenylephrine was separated on a CHIRALPAK CBH HPLC column (100 × 3 mm inner dimensions, 5 µm particle size; Sigma-Aldrich) with a mobile phase of 10 mM ammonium acetate (pH 5.8) supplemented with 10 % (v/v) 2-propanol. Chromatography was carried out at 22 °C with a flow rate of 300 µl/min. Salbutamol and terbutaline were analysed on an Astec chirobiotic T column (150 × 2.1 mm, 5 µm particle size; Sigma-Aldrich) with the corresponding guard column. For salbutamol separation, 20 mM ammonium acetate (pH 4.5) supplemented with 95 % (v/v) methanol was used as mobile phase. Flow rate was set to 400 µl/min and column temperature was kept at 40 °C for both substances. The order of elution of salbutamol enantiomers was obtained from available reference literature [40]. For norphenylephrine and terbutaline, no order of elution was available, and the enantiomers only termed as E1 and E2 for the first and second eluting enantiomer, respectively.

2.9. Calculations

Uptake ratios were determined as fold-increase in uptake into transporter-overexpressing cells over empty-vector transfected controls. For concentration-dependent uptake experiments, net uptake of OCT3 was calculated by subtraction of total uptake into empty-vector transfected cells from total uptake in OCT3-overexpressing cells. Net uptake was then plotted against the substrate concentration [S] and analyzed by

non-linear regression following the Michaelis-Menten equation with $v = v_{max} \times [S]/(K_m + [S])$ using GraphPad Prism (Version 5.01 for Windows, GraphPad Software, La Jolla, CA, USA). V_{max} is the maximum transport velocity, K_m defines the substrate concentration required to reach half v_{max}. The intrinsic clearance Cl_{int} is defined as ratio of v_{max} over K_m.

For inhibition analysis, transporter activity was calculated as according to the following formula:

$$\%\,\text{OCT3 activity} = \frac{[\text{Substrate}_{\text{inhibited}}] - [\text{Substrate}_{\text{EV}}]}{[\text{Substrate}_{\text{non-inhibited}}] - [\text{Substrate}_{\text{EV}}]}$$

$\text{Substrate}_{\text{inhibited}}$ is the uptake of ASP^+ into transporter-overexpressing cells in presence of an inhibitor whereas $\text{substrate}_{\text{non-inhibited}}$ describes the ASP^+ uptake without co-incubation with an inhibitor. $\text{Substrate}_{\text{EV}}$ refers to the passive ASP^+ uptake into empty-vector transfected control cells. Percent inhibition values where then calculated as in the following:

$$\%\,\text{transporter inhibition} = 100\% - \text{transporter activity}$$

For analysis of concentration-dependent inhibition experiments, the transporter activity was plotted against the $\log_{10}$ of inhibitor concentrations. The data was then fitted by the following formula to determine IC50 values:

$$Y = Y_{min} + \frac{(Y_{max} - Y_{min})}{1 + 10^{\log_{10}(IC50 - x) \bullet \text{Hill slope}}}$$

Y is to the transporter activity, whereas Y_{max} refers to the maximum and Y_{min} to the minimal transporter activity. X is the $\log_{10}$ of inhibitor concentrations, IC_{50} characterizes the half-maximal inhibitory concentration, and hill slope describes the slope factor. The regression was done using GraphPad Prism (Version 5.01 for Windows, GraphPad Software).

3. Results

3.1. Generation of transporter mutants

OCT3 variants were constructed by site-directed mutagenesis and stably transfected for functional characterization. The cell clones selected for functional experiments showed genomic integration of a single copy expression plasmid (Fig. 2B) and similar mRNA gene expression (Fig. 2C). When analyzing the subcellular localization with eGFP-OCT3 constructs, the E232Q, E459Q, and D478N showed severely impaired membrane localization and were retained mainly in cytoplasmic compartments (Fig. 2D). Nevertheless, we also performed transport experiments in these cell lines, although, based on our transport assays, we cannot assess if the substrates are interacting with the altered amino acid during the translocation, i.e. if the mutated amino acid has a substrate-specific function.

The functional (transport and transport inhibition) experiments were performed with HEK293 cells overexpressing wild type and mutant OCT3 (without the eGFP). In the following, first, the effects of removing the negative charges in the presumed substrate translocation path are described concerning transport activity and then concerning susceptibility to inhibition.

3.2. Uptake of fluorescent ASP^+ and other typical OCT3 substrates

For all generated mutants, the uptake of the OCT model substrate ASP^+ were analysed (Fig. 3). E390Q showed negligible net uptake of ASP^+, which was reflected by overall low intrinsic clearances for ASP^+

Table 2
Kinetic parameters of ASP^+ transport by wild-type and mutated OCT3.

OCT3 Mutation	V_{max} (±SEM) [pmol × mg protein^{-1} × min^{-1}]	K_M (±SEM) [μM]	Cl_{int} (±SEM) [μL × mg protein^{-1} × min^{-1}]	Subcellular Localization
WT	6410 ± 854	82.8 ± 33.7	77.4 ± 41.8	Membrane
D155N	2975 ± 382*	44.7 ± 20.7	66.6 ± 39.4	Membrane
E232Q	367 ± 282***	686 ± 859	0.53 ± 1.08	Cytosol
D382N	6078 ± 722	98.9 ± 34.35	61.5 ± 28.7	Membrane
E390Q	8.05 ± 15.9***	3.88 ± 73.4	2.08 ± 43.4	Membrane
E451Q	652 ± 44.6***	19.3 ± 6.18	33.8 ± 13.1	Membrane
E459Q	744 ± 7802	2812 ± 34720	0.26 ± 6.04	Cytosol
D478N	675 ± 172***	156 ± 103	4.32 ± 3.97	Mainly Cytosol

Asterisks indicate statistical significance of the differences between the parameters of wild type and mutant transporter (Student's *t*-test; *p < 0.05, **p < 0.01, ***p < 0.001).

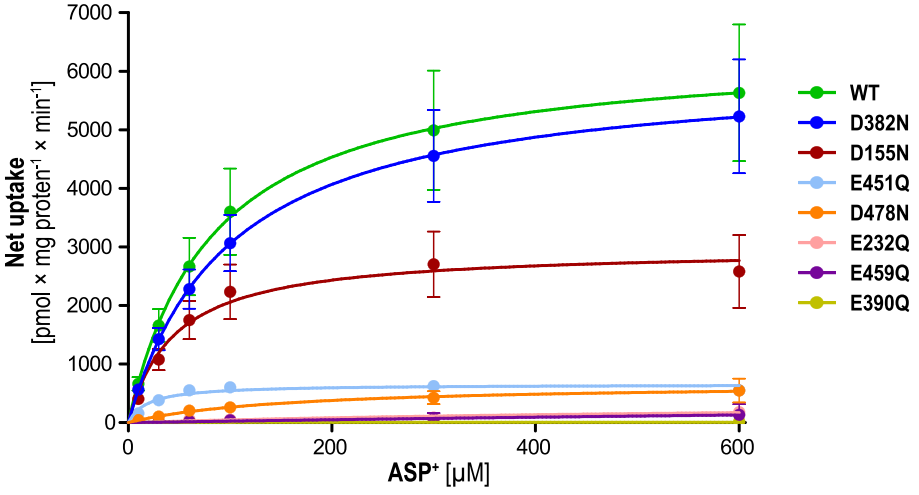

Fig. 3. Effects of mutating the negatively charged amino acids presumed to be most relevant for substrate translocation by OCT3. ASP^+ (4-(4-(dimethylamino)styryl)-N-methylpyridinium) was used as the fluorescent model substrate of OCT3. HEK293 cells overexpressing wild type OCT3, generated mutants and empty-vector transfected control cells were incubated with increasing concentrations of ASP^+ for 2 min. Intracellular ASP^+ was then quantified by fluorescence measurement. Shown is the net uptake of three independent experiments as mean ± SEM.

transport compared to the wild-type variant (Table 2). Similarly, the uptake by E232Q, E459Q, and D478N was minor, which was expected as a consequence of improper membrane localization.

The D382N mutant of OCT3 showed wild type-like transport of ASP^+. In contrast, mutation of D155 resulted in reduced transport of activity to almost 50 %. The E451Q mutant showed even more strongly reduced transport and reached only 10 % of the transporter capacity of wild type OCT3.

To analyse whether the functional effects of the introduced mutations may be substrate-dependent, we further investigated the uptake of 15 structurally diverse OCT3 substrates (Fig. 4). Like the ASP^+ transport, E232Q, E390Q, E459Q, and D478N showed almost no uptake of the tested substrates (Fig. 4B). Among those, only the D478N mutant showed relevant uptake of MPP^+ and *meta*-Iodobenzylguanidine. However, uptake ratios for both were still only at 23 % and 16 % of the wild-type uptake, respectively. The D382N mutant showed uptake ratios similar to wild-type OCT3; only methylnaltrexone was less efficiently transported by the D382N mutant.

Interestingly, D155N and E451Q had strong substrate-specific effects (Fig. 4A). In particular, uptake via the D155N variant ranged from full wild-type-like activity for histamine and MPP^+ to a complete lack of transport for emtricitabine, thiamine and terbutaline. Also, transport via the E451Q variant differed strongly for the investigated substrates. Benzyltriethylammonium, MPP^+ and salbutamol were transported almost with full activity, whereas other substrates such as famotidine and methacholine showed only 9 % and 11 % uptake of the wild type, respectively. Among the racemic substrates, norphenylephrine showed no stereoselective uptake whereas salbutamol and terbutaline were transported stereoselectively. This was not changed for the mutants with remaining activity except for E451Q, which showed total selectivity for terbutaline transport with no net uptake of the second enantiomer.

3.3. Inhibition of ASP^+ by structurally diverse inhibitors

To test whether the mutated residues might also affect the binding of OCT3 inhibitors, we analyzed the inhibition of OCT3 variants by several substances at a single concentration using ASP^+ as a model substrate (Fig. 5A). In addition, we characterized inhibition potencies of the well-established OCT3 inhibitors corticosterone and decynium-22 (Fig. 5B). We could only investigate those OCT3 variants which showed relevant ASP^+ transport activity – D155N and D382N. Inhibition studies with E451Q using ASP^+ as model substrate were not possible due to insufficient ASP^+ uptake.

The D155N mutant was inhibited more strongly than the wild type. This was reflected by 4.6- and 3.6-fold lower IC_{50} values for corticosterone and decynium-22, respectively (Table 3), but also by the inhibition data for a single concentration by 20 additional substances. For D382, inhibition by corticosterone and decynium-22 differed not significantly from the inhibition of the wild-type transporter. However, the single concentration inhibition was on average less strongly compared to the wild type (Fig. 5C).

Wild-type OCT3 and both mutants showed highly stereoselective inhibition by quinine/quinidine and verapamil enantiomers in favor of quinine and *(S)*-verapamil, respectively.

4. Discussion

Negatively charged amino acids have been identified early as responsible for the interaction of positively charged substrates of organic cation transporters [1]. Out of those, the conserved D478 (numbering consistent with hOCT3) in OCTs was the main center of attention [27] until the recently published cryo-EM structures-guided experimental studies on OCT1 [30] revealed an even more critical role of E386 (E390 for OCT3) for the transport of different substrates.

In our study, we could demonstrate that, also for OCT3, E390 seems to be a most important anionic amino acid for transporting cationic substrates. Despite correct membrane localization of the E390Q mutant, all tested substrates showed no remaining transport activity (Fig. 4B). This was expected given the high homology of OCT3 to OCT1 with about 50 % amino acid identity [41]. Although there is no experimental proof available yet, it appears very likely that this amino acid might then also crucial for the function of OCT2 since it is conserved for all three OCTs. However, since this glutamic acid residue is also conserved for the OCTNs and a negatively charged amino acid is also located at this position for the OATs (Fig. 1B), it might be interesting to study the function of this residue for the transport of organic anions via those transporters. Right now, there is no functional data available for the OCTNs and OATs but computational modelling suggests indeed a relevant role of the corresponding E381 in OCTN1, but so far only for interaction with the positive charged nitrogen in carnitine and tetraethylammonium but also for the interaction with sodium ions [42].

E232 and E459 are not only conserved among the three OCTs, but also for OCTNs and the OATs (Fig. 1B). The here generated mutated versions of these residues led to an impairment of the subcellular localization and were strongly retained in cytoplasmatic compartments (Fig. 2D). Accordingly, E232 and E459 seem to have a critical role in protein folding and, based on our data, we can neither proof nor exclude that they might be also involved in transporter-ligand interactions. Unexpectedly, the D478N mutant showed also a strongly impaired membrane localization which is in contrast to the corresponding D474N mutant of OCT1 which showed proper localization previously [5]. Nevertheless, the here generated D478N mutant showed uptake of MPP^+ and *meta*-iodobenzylguanidine which indicates that a minor portion of the transporter might still reach the plasma membrane.

The probably most interesting insights from our study might be the substrate-specific effects of D155N and E451Q mutants. Both amino acids have been rarely studied in the context of organic cation transporters. Only for the E451Q mutant in OCT3, a stronger inhibition of MPP^+ uptake has been described for several polyamines such as spermine and spermidine [43]. Here we could show that transport activity varied strongly for different substrates and ranged from full transport activity to almost no uptake (Fig. 4). This further substantiates what was proposed by the recent cryo-EM studies [30] that polyspecific transport by OCTs might be achieved by substrate binding to an orthosteric site, which is formed by E390 together with several aromatic amino acids, and several opportunistic binding sites which are only engaged by distinct substrates. E451Q might be an integral part of such an opportunistic binding site.

The limited number of investigated substrates limits conclusions regarding molecular features of ligands which might engage this binding site. Nevertheless, transport was mostly reduced for large substrates such as famotidine, methylnaltrexone, and thiamine. Based on their size, it is reasonable that parts of the molecules interact with other sites within the transporters binding pocket in addition to the orthosteric site around E390. D155 is located rather at the entrance to the substrate binding pocket (Fig. 1A) and could therefore function as first contact of a substrate or an inhibitor with the transporter, before the substrates engages the main binding site required for translocation. The affinity to all inhibitors was increased in the D155N mutant (Fig. 5A and B). As expressed by the IC50 values, the elimination of the negative charge at OCT3 codon 155 increased affinity to corticosterone by about 4.5-fold and to decynium 22 by about 3.5-fold (Table 3). This is plausible considering that D155 is localized at the entrance site of the protein ([29] supplementary Figure 11) and the negative charge of aspartic acid 155 might even decrease access for both inhibitors to their optimum binding site or weaken their binding.

The D382N mutant showed no altered transport compared to the wild type (Fig. 4). However, several non-transported inhibitors such as chlorhexidine, cimetidine, and crizotinib showed reduced inhibition compared to the wild type (Fig. 5C). Accordingly, even though this amino acid seems to be not involved in the interaction with the here tested substrates, it might be important for the binding of certain

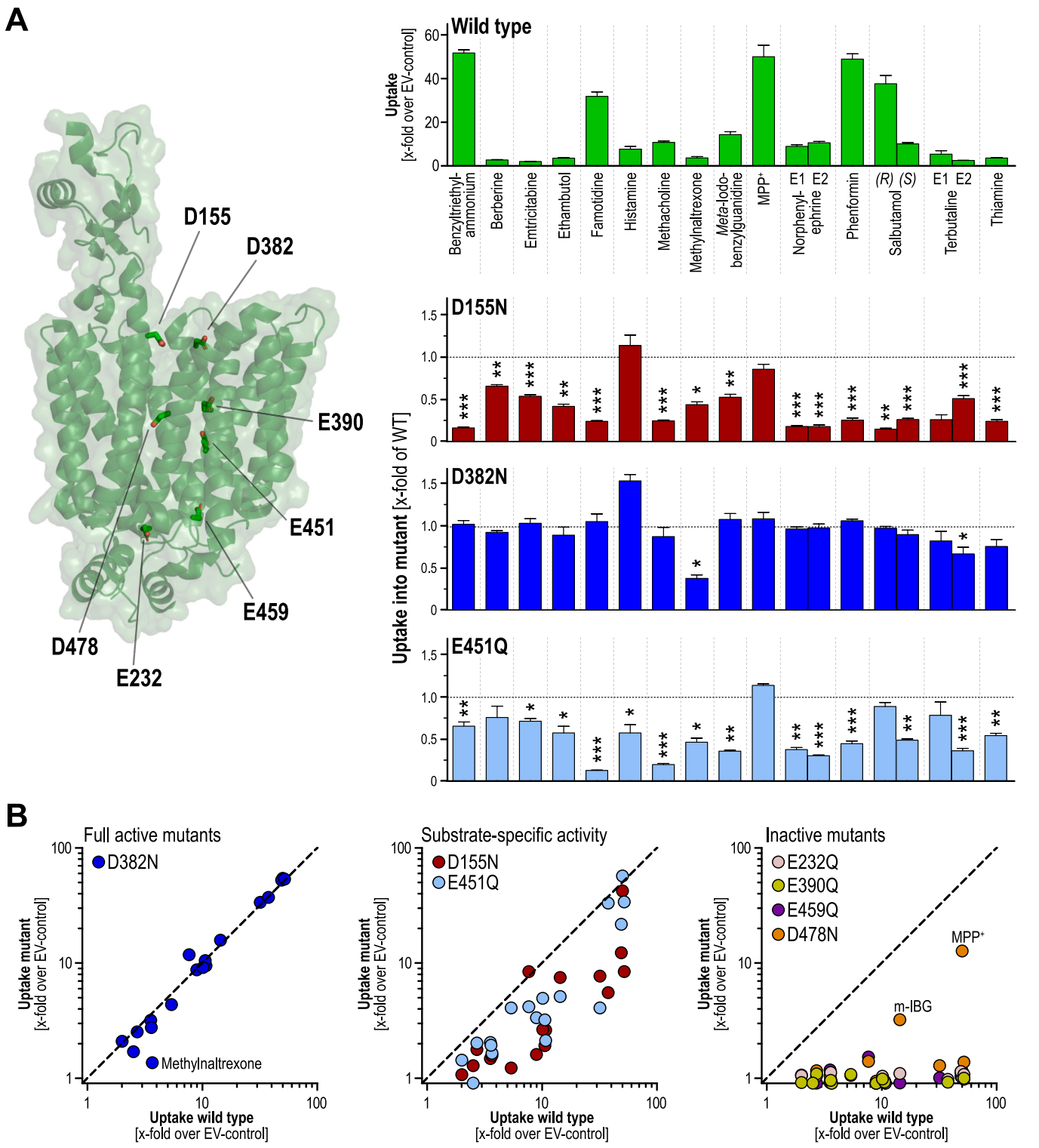

Fig. 4. Differential uptake of structurally diverse substrates by OCT3 mutants. A: Localization of the studied negatively charged amino acids in the OCT3 structure [29] and substrate-dependent effects of the D155, D382, and E451 "neutralization". HEK293 cells overexpressing wild-type OCT3, generated mutants and empty-vector transfected control cells were incubated with 2.5 μM substrate for 2 min. Intracellular substrate concentration was quantified by HPLC-MS/MS analysis. Uptake in wild-type OCT3 is expressed as the fold-increase in transporter-overexpressing cells over empty vector (EV)-transfected control and represented as mean ± SEM of three independent experiments. Activity in the 3 mutants shown below is expressed relative to the activities of wild-type OCT3. Asterisks indicate statistical significance of the differences between the uptake ratio of wild type and mutant transporters (Student's *t*-test; *p < 0.05, **p < 0.01, ***p < 0.001). As illustrated, with almost all substrates, the D155N and E451Q variants resulted in (differently strong) reduction of transport activity. With some exceptions, the wild-type transport activity was maintained in the D382N mutation. **B:** Correlation of uptake data for full active, substrate-specific and inactive mutants. Mutant uptake ratios are shown on the Y-axis, whereas uptake of the wild-type transporter is shown on the X-axis. The dashed lines indicate the bisection and equal transport.

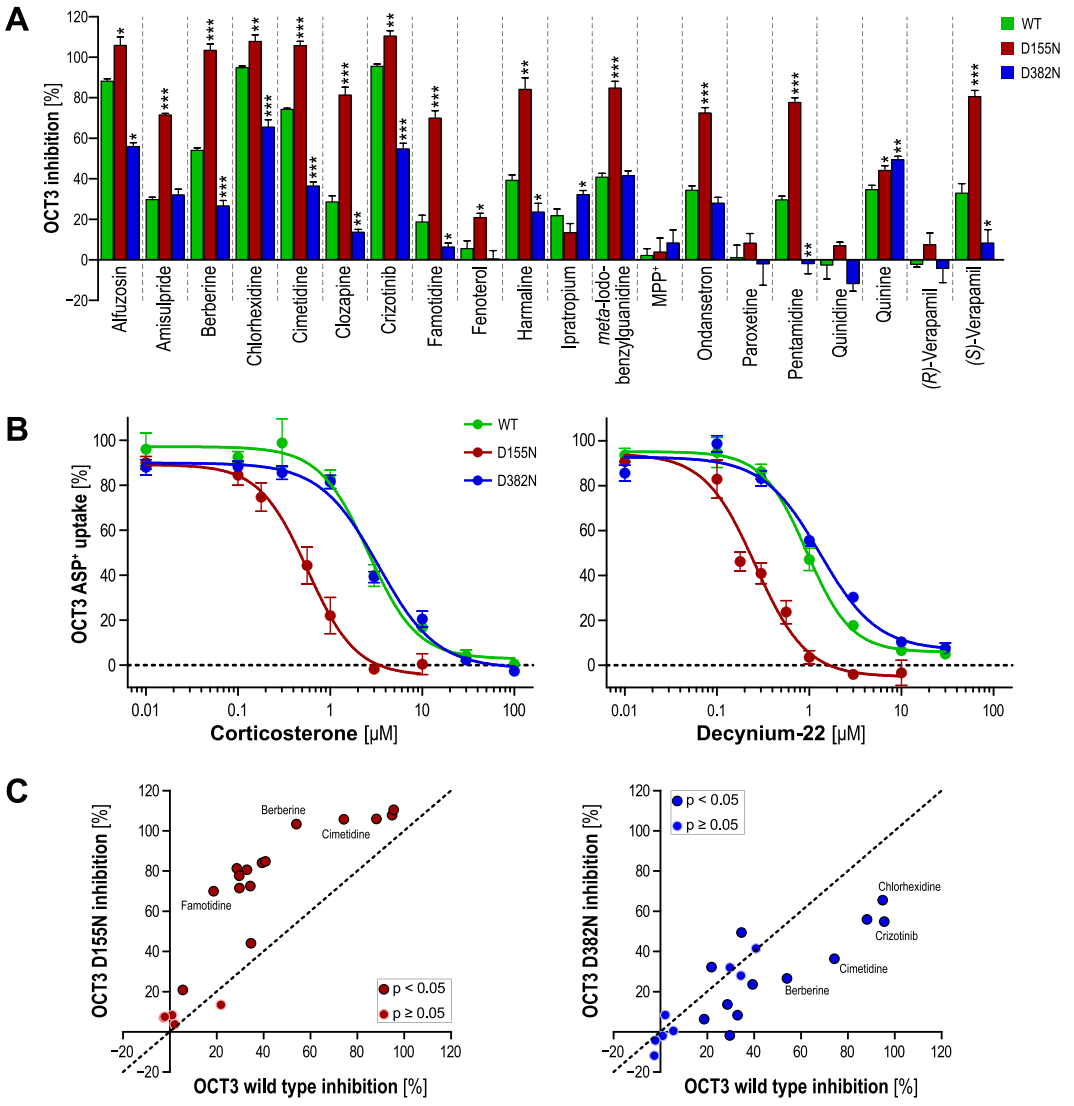

Fig. 5. OCT3 inhibition and comparison to D155N and D382N mutants. A: HEK293 cells overexpressing wild-type OCT3, generated mutants and empty-vector transfected control cells were incubated with 2 µM ASP^+ and a single concentration of 20 µM substrate or increasing concentrations of corticosterone and decynium-22 (panel **B**) for 5 min. Intracellular ASP^+ was then quantified by fluorescence measurement. Data is presented as mean ± SEM of three independent experiments. Asterisks indicate statistical significance of the differences between the inhibition of the wild type and mutant transporters (Student's *t*-test; *p < 0.05, **p < 0.01, ***p < 0.001). **C:** Correlation of inhibition data. The dashed line indicates the bisection and, thereby equal transporter inhibition. Statistical significance in the inhibition of the wild-type and mutant transporters was determined by Student's *t* test.

Table 3
IC_{50} of corticosterone and decynium-22 inhibition of OCT3.

OCT3 Mutation	IC_{50} (95 % confidence intervals) [µM]	
	Corticosterone	Decynium-22
WT	2.60 (1.95 to 3.46)	0.941 (0.745 to 1.19)
D155N	0.570 (0.397 to 0.818)	0.261 (0.189 to 0.361)
D382N	3.34 (2.58 to 4.34)	1.31 (1.00 to 1.71)

inhibitors.

A final consideration might be to what extent the insights we obtained here for OCT3 might be translatable onto the related OCT1 or OCT2. In a recent work, the full landscape of OCT1 mutations was created by characterizing the functional impact of all possible mutations [44]. Many of our conclusions for OCT3 were also demonstrated for OCT1 (Table 4). Moreover, the authors provide several, reasonable explanations for the phenotypes we observed here for OCT3. For the D149N mutant in OCT1 (corresponds to D155N in OCT3), molecular dynamics simulations suggested a severe destabilization of the cycling of the transporter between outward and inward states, thereby limiting efficient substrate translocation. This is well reflected by our data for OCT3, since the D155N mutant showed a substrate-dependent reduction of transporter but not a complete loss of activity (Fig. 4). Interestingly, for E226 and E455 in OCT1 (correspond to E232 and E459 in OCT3, respectively), the authors proposed critical functions for protein folding. This aligns well with the impaired membrane localization of the respective generated OCT3 mutants in our study (Fig. 2D). Finally, they also highlight the critical role of E386 in OCT1 (corresponds to E390 in OCT3) for substrate interaction and any mutation at this position (except E386D) resulted in almost complete loss of transport activity, which we could also observe for the OCT3 E390Q mutant.

Altogether, our study complements the insights recently gained by cryo-EM studies on a biochemical level, and moreover, transferred many insights so far known for OCT1 towards OCT3. Our study also shows that testing structurally different substrates, as done here, on generated transporter mutants might be important to further decipher the polyspecific nature of organic cation transporters.

Table 4
Summary and comparison of OCT3 mutagenesis data to OCT1 mutagenesis data from Yee et al. [44].

Mutation OCT3	Membrane localization	Functional effects	Homologous OCT1 amino acid	Functional effects in OCT1 according to data of Yee et al. [44]
D155N	Normal	Substrate-dependent effects; increased affinity to all inhibitors tested	D149	Correct membrane localization of D149N, mild uptake impairment
E232Q	Deficient	No transport	E226	Critical role in protein folding, all possible mutations led to strongly reduced uptake
D382N	Normal	Normal activity (except methylnaltrexone); same or decreased affinity to inhibitors	D378	No strong phenotype for any possible mutation
E390Q	Normal	No transport	E386	Correct membrane localization of E386Q, Strongly reduced uptake for all possible mutations
E451Q	Normal	Substrate-dependent effects	Not conserved	–
E459Q	Deficient	No transport	E455	Critical role in protein folding, all possible mutations led to strongly reduced uptake
D478N	Reduced	No transport except for MPP^+ and m-IBG	D474	All possible mutations led to strongly reduced uptake

CRediT authorship contribution statement

Kyra-Elisa M. Redeker: Conceptualization, Investigation, Visualization, Writing – original draft, Writing – review & editing. **Sophie Schröder:** Investigation, Resources, Visualization, Writing – original draft. **Christof Dücker:** Conceptualization, Visualization, Writing – original draft. **Jürgen Brockmöller:** Conceptualization, Funding acquisition, Resources, Writing – review & editing. **Lukas Gebauer:** Conceptualization, Investigation, Visualization, Writing – original draft, Writing – review & editing.

Declaration of competing interest

The authors declare that they have no known competing financial interests or personal relationships that could have appeared to influence the work reported in this paper.

Data availability

Data will be made available on request.

Acknowledgements

We would like to thank Ellen Bruns for her excellent technical assistance with chiral HPLC analysis and Chemaxon (Budapest, Hungary) for generously providing the academic license for MarvinSketch and the Instant JChem Suite. This study was funded by the Deutsche Forschungsgemeinschaft (DFG, German Research Foundation) – grant ID 461080000 and the research program of the University Medical Center, University of Göttingen. We acknowledge support by the Open Access Publication Funds/transformative agreements of the Göttingen University.

References

[1] H. Koepsell, Organic cation transporters in health and disease, Pharmacol. Rev. 72 (1) (2020) 253–319.
[2] R. Hendrickx, J.G. Johansson, C. Lohmann, R.-M. Jenvert, A. Blomgren, L. Börjesson, L. Gustavsson, Identification of novel substrates and structure-activity relationship of cellular uptake mediated by human organic cation transporters 1 and 2, J. Med. Chem. 56 (18) (2013) 7232–7242.
[3] O. Jensen, L. Gebauer, J. Brockmöller, C. Dücker, Relationships between inhibition, transport and enhanced transport via the organic cation transporter 1, Int. J. Mol. Sci. 23 (4) (2022) 2007.
[4] L. Gebauer, O. Jensen, J. Brockmöller, C. Dücker, Substrates and inhibitors of the organic cation transporter 3 and comparison with OCT1 and OCT2, J. Med. Chem. 65 (18) (2022) 12403–12416.
[5] K.-E.-M. Redeker, O. Jensen, L. Gebauer, M.J. Meyer-Tönnies, J. Brockmöller, Atypical substrates of the organic cation transporter 1, Biomolecules 12 (11) (2022) 1664.
[6] C. Hilgendorf, G. Ahlin, A. Seithel, P. Artursson, A.L. Ungell, J. Karlsson, Expression of thirty-six drug transporter genes in human intestine, liver, kidney, and organotypic cell lines, Drug Metab. Dispos. 35 (8) (2007) 1333–1340.
[7] A.T. Nies, H. Koepsell, S. Winter, O. Burk, K. Klein, R. Kerb, U.M. Zanger, D. Keppler, M. Schwab, E. Schaeffeler, Expression of organic cation transporters OCT1 (SLC22A1) and OCT3 (SLC22A3) is affected by genetic factors and cholestasis in human liver, Hepatology (Baltimore Md.) 50 (4) (2009) 1227–1240.
[8] H. Motohashi, Y. Sakurai, H. Saito, S. Masuda, Y. Urakami, M. Goto, A. Fukatsu, O. Ogawa, K.I. Inui, Gene expression levels and immunolocalization of organic ion transporters in the human kidney, J. Am. Soc. Nephrol. 13 (4) (2002) 866–874.
[9] X. Wu, R. Kekuda, W. Huang, Y.J. Fei, F.H. Leibach, J. Chen, S.J. Conway, V. Ganapathy, Identity of the organic cation transporter OCT3 as the extraneuronal monoamine transporter (uptake2) and evidence for the expression of the transporter in the brain, J. Biol. Chem. 273 (49) (1998) 32776–32786.
[10] T.F. Solbach, M. Grube, M.F. Fromm, O. Zolk, Organic cation transporter 3: expression in failing and nonfailing human heart and functional characterization, J. Cardiovasc. Pharmacol. 58 (4) (2011) 409–417.
[11] M.A. Selo, J.A. Sake, C. Ehrhardt, J.J. Salomon, Organic cation transporters in the lung—current and emerging (patho)physiological and pharmacological concepts, Int. J. Mol. Sci. 21 (23) (2020) 9168.
[12] V. Vialou, L. Balasse, J. Callebert, J.M. Launay, B. Giros, S. Gautron, Altered aminergic neurotransmission in the brain of organic cation transporter 3-deficient mice, J. Neurochem. 106 (3) (2008) 1471–1482.
[13] Y. Wang, Q. Shi, M. Li, M. Zhao, R. Reddy Gopireddy, J.P. Teoh, B. Xu, C. Zhu, K. E. Ireton, S. Srinivasan, S. Chen, P.J. Gasser, J. Bossuyt, J.W. Hell, D.M. Bers, Y. K. Xiang, Intracellular β(1)-adrenergic receptors and organic cation transporter 3 mediate phospholamban phosphorylation to enhance cardiac contractility, Circ. Res. 128 (2) (2021) 246–261.
[14] W. Song, Q. Luo, Y. Zhang, L. Zhou, Y. Liu, Z. Ma, J. Guo, Y. Huang, L. Cheng, Z. Meng, Organic cation transporter 3 (Oct3) is a distinct catecholamines clearance route in adipocytes mediating the beiging of white adipose tissue, PLoS Biol. 17 (1) (2019) e2006571.
[15] J. Vollmar, Y.O. Kim, J.U. Marquardt, D. Becker, P.R. Galle, D. Schuppan, T. Zimmermann, Deletion of organic cation transporter Oct3 promotes hepatic fibrosis via upregulation of TGFβ, American journal of physiology, Gastrointestinal and Liver Physiology 317 (2) (2019) G195–G202.
[16] M. Heise, A. Lautem, J. Knapstein, J.M. Schattenberg, M. Hoppe-Lotichius, D. Foltys, N. Weiler, A. Zimmermann, A. Schad, D. Gründemann, G. Otto, P. R. Galle, M. Schuchmann, T. Zimmermann, Downregulation of organic cation transporters OCT1 (SLC22A1) and OCT3 (SLC22A3) in human hepatocellular carcinoma and their prognostic significance, BMC Cancer 12 (2012) 109.
[17] L.E. Honan, R. Fraser-Spears, L.C. Daws, Organic cation transporters in psychiatric and substance use disorders, Pharmacol. Ther. 108574 (2023).
[18] H. Koepsell, Multiple binding sites in organic cation transporters require sophisticated procedures to identify interactions of novel drugs, Biol. Chem. 400 (2) (2019) 195–207.
[19] L. Gebauer, N. Arul Murugan, O. Jensen, J. Brockmöller, M. Rafehi, Molecular basis for stereoselective transport of fenoterol by the organic cation transporters 1 and 2, Biochem. Pharmacol. 197 (2022) 114871.
[20] V. Gorboulev, N. Shatskaya, C. Volk, H. Koepsell, Subtype-specific affinity for corticosterone of rat organic cation transporters rOCT1 and rOCT2 depends on three amino acids within the substrate binding region, Mol. Pharmacol. 67 (5) (2005) 1612–1619.
[21] C. Volk, V. Gorboulev, A. Kotzsch, T.D. Müller, H. Koepsell, Five amino acids in the innermost cavity of the substrate binding cleft of organic cation transporter 1 interact with extracellular and intracellular corticosterone, Mol. Pharmacol. 76 (2) (2009) 275–289.
[22] C. Popp, V. Gorboulev, T.D. Müller, D. Gorbunov, N. Shatskaya, H. Koepsell, Amino acids critical for substrate affinity of rat organic cation transporter 1 line the substrate binding region in a model derived from the tertiary structure of lactose permease, Mol. Pharmacol. 67 (5) (2005) 1600–1611.

[23] M.J. Meyer, M.V. Tzvetkov, OCT1 polyspecificity—friend or foe? Front. Pharmacol. 12 (2021).
[24] V. Gorboulev, S. Rehman, C.M. Albert, U. Roth, M.J. Meyer, M.V. Tzvetkov, T. D. Mueller, H. Koepsell, Assay conditions influence affinities of rat organic cation transporter 1: analysis of mutagenesis in the modeled outward-facing cleft by measuring effects of substrates and inhibitors on initial uptake, Mol. Pharmacol. 93 (4) (2018) 402–415.
[25] G. Dmitry, G. Valentin, S. Natalia, M. Thomas, B. Ernst, F. Thomas, K. Hermann, High-affinity cation binding to organic cation transporter 1 induces movement of Helix 11 and blocks transport after mutations in a modeled interaction domain between two helices, Mol. Pharmacol. 73 (1) (2008) 50.
[26] E. Andreev, N. Brosseau, E. Carmona, A.-M. Mes-Masson, D. Ramotar, The human organic cation transporter OCT1 mediates high affinity uptake of the anticancer drug daunorubicin, Sci. Rep. 6 (1) (2016) 20508.
[27] V. Gorboulev, C. Volk, P. Arndt, A. Akhoundova, H. Koepsell, Selectivity of the polyspecific cation transporter rOCT1 is changed by mutation of aspartate 475 to glutamate, Mol. Pharmacol. 56 (6) (1999) 1254–1261.
[28] T. Keller, V. Gorboulev, T.D. Mueller, V. Dötsch, F. Bernhard, H. Koepsell, Rat organic cation transporter 1 contains three binding sites for substrate 1-Methyl-4-phenylpyridinium per monomer, Mol. Pharmacol. 95 (2) (2019) 169–182.
[29] B. Khanppnavar, J. Maier, F. Herborg, R. Gradisch, E. Lazzarin, D. Luethi, J.-W. Yang, C. Qi, M. Holy, K. Jäntsch, O. Kudlacek, K. Schicker, T. Werge, U. Gether, T. Stockner, V.M. Korkhov, H.H. Sitte, Structural basis of organic cation transporter-3 inhibition, Nat. Commun. 13 (1) (2022) 6714.
[30] Y. Suo, N.J. Wright, H. Guterres, J.G. Fedor, K.J. Butay, M.J. Borgnia, W. Im, S.-Y. Lee, Molecular basis of polyspecific drug and xenobiotic recognition by OCT1 and OCT2, Nat. Struct. Mol. Biol. 30 (7) (2023) 1001–1011.
[31] Y.C. Zeng, M. Sobti, A. Quinn, N.J. Smith, S.H.J. Brown, J.I. Vandenberg, R. M. Ryan, M.L. O'Mara, A.G. Stewart, Structural basis of promiscuous substrate transport by organic cation transporter 1, Nat. Commun. 14 (1) (2023) 6374.
[32] The UniProt Consortium, UniProt: the universal protein knowledgebase in 2023, Nucleic Acids Res. 51 (D1) (2023) D523–D531.
[33] R.C. Edgar, MUSCLE: multiple sequence alignment with high accuracy and high throughput, Nucleic Acids Res. 32 (5) (2004) 1792–1797.
[34] A.M. Waterhouse, J.B. Procter, D.M.A. Martin, M. Clamp, G.J. Barton, Jalview version 2—a multiple sequence alignment editor and analysis workbench, Bioinformatics 25 (9) (2009) 1189–1191.
[35] O. Edelheit, A. Hanukoglu, I. Hanukoglu, Simple and efficient site-directed mutagenesis using two single-primer reactions in parallel to generate mutants for protein structure-function studies, BMC Biotech. 9 (1) (2009) 61.
[36] A.R. Saadatmand, S. Tadjerpisheh, J. Brockmöller, M.V. Tzvetkov, The prototypic pharmacogenetic drug debrisoquine is a substrate of the genetically polymorphic organic cation transporter OCT1, Biochem. Pharmacol. 83 (10) (2012) 1427–1434.
[37] K.J. Livak, T.D. Schmittgen, Analysis of relative gene expression data using real-time quantitative PCR and the 2(-Delta Delta C(T)) Method, Methods (San Diego, Calif.) 25 (4) (2001) 402–408.
[38] P.K. Smith, R.I. Krohn, G.T. Hermanson, A.K. Mallia, F.H. Gartner, M. D. Provenzano, E.K. Fujimoto, N.M. Goeke, B.J. Olson, D.C. Klenk, Measurement of protein using bicinchoninic acid, Anal. Biochem. 150 (1) (1985) 76–85.
[39] L. Gebauer, O. Jensen, M. Neif, J. Brockmöller, C. Dücker, Overlap and specificity in the substrate spectra of human monoamine transporters and organic cation transporters 1, 2, and 3, Int. J. Mol. Sci. (2021).
[40] A. Halabi, C. Ferrayoli, M. Palacio, V. Dabbene, S. Palacios, Validation of a chiral HPLC assay for (R)-salbutamol sulfate, J. Pharm. Biomed. Anal. 34 (1) (2004) 45–51.
[41] V. Gorboulev, J.C. Ulzheimer, A. Akhoundova, I. Ulzheimer-Teuber, U. Karbach, S. Quester, C. Baumann, F. Lang, A.E. Busch, H. Koepsell, Cloning and characterization of two human polyspecific organic cation transporters, DNA Cell Biol. 16 (7) (1997) 871–881.
[42] L. Pochini, F. Barone, L. Console, C. Brunocilla, M. Galluccio, M. Scalise, C. Indiveri, OCTN1 (SLC22A4) displays two different transport pathways for organic cations or zwitterions, Biochimica et Biophysica Acta (BBA) Biomembranes (2023) 184263.
[43] D.C. Li. Pharmacology of Organic Cation Transporters: Focus on Structure-Function Relationships in OCT3 (SLC22A3), Undergraduate Theses—Unrestricted. 29, 2015.
[44] S.W. Yee, C. Macdonald, D. Mitrovic, X. Zhou, M.L. Koleske, J. Yang, D.B. Silva, P. R. Grimes, D. Trinidad, S.S. More, L. Kachuri, J.S. Witte, L. Delemotte, K. M. Giacomini, W. Coyote-Maestas, The full spectrum of OCT1 (SLC22A1) mutations bridges transporter biophysics to drug pharmacogenomics, bioRxiv - the preprint server for biology (2023), https://doi.org/10.1101/2023.06.06.54396.